

Diffusionlike Drying of a Nanoporous Solid as Revealed by Magnetic Resonance Imaging

Benjamin Maillet¹,²,³,⁴ Guido Dittrich²,³,⁴ Patrick Huber^{2,3,4} and Philippe Coussot^{1,*}

¹Laboratoire Navier (Ecole des Ponts Paris Tech-Univ Gustave Eiffel-CNRS), Champs-sur-Marne, France

²Institute for Materials and X-Ray Physics, Hamburg University of Technology, Hamburg, Germany

³Center for X-Ray and Nano Science CXNS, Deutsches Elektronen-Synchrotron DESY, Hamburg, Germany

⁴Center for Hybrid Nanostructures CHyN, University Hamburg, Hamburg, Germany

 (Received 24 June 2022; revised 2 September 2022; accepted 11 October 2022; published 9 November 2022)

Drying plays a central role in various fabrication processes and applications of functional nanoporous materials, most prominently in relation to energy storage and conversion. During such processes, liquid coexists with air inside the sample, leading to transport as a result of concentration gradients of vapor and/or liquid. Experimentally, it is extremely challenging to unravel this transport phenomenology inside the hidden geometry of porous media. Here, we observe the drying of a model nanoporous material (monolithic mesoporous silica glass, Vycor) with magnetic resonance imaging. We show that, for various boundary conditions (air-flux intensities), no dry region develops, but the sample desaturates in depth. This desaturation is almost homogeneous throughout the sample for weak air flux, while saturation gradients can be observed for sufficiently strong air flux. We demonstrate that the transport of water is mainly ensured by liquid flow towards the free surface, resulting from a gradient of vapor pressure, associated with local saturation (via the desorption curve), leading to a gradient of liquid pressure (via the Kelvin law). Assuming otherwise standard hydrodynamic characteristics of the nanoconfined liquid, this results in a diffusionlike model, which appears to represent experimental data very well in terms of the spatial distribution of water over time inside the sample for various boundary conditions (air-flux intensities). Finally, we propose a predictive model of the detailed drying characteristics of a nanomaterial from knowledge of its pore size, permeability, and desorption curve. This provides an insight into the rational design of drying-based processes employing functional nanoporous materials and allows for a mechanistic understanding of drying phenomenologies in natural nanoporous media.

DOI: [10.1103/PhysRevApplied.18.054027](https://doi.org/10.1103/PhysRevApplied.18.054027)

I. INTRODUCTION

Water transport in nanoporous media plays a central role in many aspects of science and technology: shrinkage or cracks during drying of clay, nanocolloidal gels [1,2], or cement [3]; moisture transfer in cementitious construction materials [4] and its impact on durability or building comfort and heating [5]; hydrocarbon release in low-permeability reservoirs [6]; sap flow in plants [7,8]; and the synthesis of and *in operando* performance of the wide class of functional nanoporous materials [9,10]. Also, considering the latent heat associated with liquid-vapor transition, water sorption or desorption might constitute a source of energy storage or harvesting and is already of crucial importance in many technical cooling applications, most prominently the cooling of electronic devices [10]. Also, capillary forces in pore space emerging upon

drying can be used as bioinspired mechanical actuation schemes [11–13].

The extraction of liquid from nanoporous systems can involve some liquid flow, but the nanofluidic behavior of liquids confined in nanopores is a subject of debate [14,15]; the main questions are whether continuum fluid mechanics still applies when the pore scale is not much larger than the molecular size, and if the viscous fluid properties are similar. One nanometer is considered to be the critical size, below which continuum mechanics does not apply anymore, but various specific effects can occur just above this limit [16]. For example, it was proposed that standard hydraulic laws applied if one took into account a slipping [17] or fixed molecular layer [18–20]. Also, the usual capillary imbibition process [21] was shown to follow the same rules at the nanoscale [8,22,23].

The desorption case is *a priori* more complex, as now one can expect the coexistence of water and air in nanopores at different stages of the process, with questions about the interactions between the liquid, the vapor,

*Philippe.coussot@univ-eiffel.fr

and the solid and the resulting transport properties. More generally, there are questions about the free-surface hydrodynamics of the liquid in nanopores [24,25]. So far, most studies have focused on evaporation from one-dimensional (1D) or two-dimensional nanoporous systems, for which the liquid-air interface was fixed [26–28] or observable [29–31], so that the process could essentially be described by taking into account evaporation and vapor diffusion from relatively simple air-liquid interfaces. The drying of three-dimensional (3D) nanoporous systems is directly connected to various applications, but its study also constitutes a greater challenge due to the difficulty of internal visualization and theoretical description of a two-phase flow through a complex medium.

During drying of real (3D) micro- or macroporous media, pore-network effects occur that sensitively depend on geometrical parameters such as the ratio of pore length to pore diameter, tortuosity, and interconnectivity [32–34]. However, usually, they homogeneously desaturate [35–38]. This is due to dominant capillary forces, which increase when the pore size decreases, and which induce sufficiently fast equilibration of the water content (and thus, of the Laplace pressure) throughout the medium. Then, below some critical saturation (current liquid volume divided by the void volume in the absence of liquid, denoted as S) and air flux, a dry region develops from the free surface [38–40]. It is not clear whether similar effects can take place in nanoporous media, as internal observations in such systems are scarce. Magnetic resonance imaging (MRI) of drying nanocolloidal gels (made of silica beads with radii down to 6 nm) under a single air flux nevertheless shows that some saturation gradient develops from the beginning of the experiments until the end, but no dry region appears [1,38]. Thus, remarkably, such nanoporous samples are still able to desaturate in depth more or less like macroporous materials, but the exact physical origin and dynamics are not yet established.

Here, we provide a rigorous analysis of the drying of a nanoporous solid based on the analysis of NMR measurements, giving detailed information on the local liquid content at any time during water extraction from a model nanoporous material under different conditions. Through a detailed theoretical description of the physical mechanisms, we finally show that water transport is mainly ensured by liquid flow resulting from a gradient of vapor pressure, and assuming otherwise standard hydrodynamic characteristics, so that the whole process of extraction is very well described by a diffusion model with a diffusion coefficient that, as a first approximation, can be considered as constant.

II. MATERIALS AND METHODS

We use porous Vycor glass (Corning glass, code 7930), a virtually pure fused silica glass permeated by an

isotropic three-dimensional network of interconnected tortuous pores [41,42]. From the nitrogen-sorption isotherm, the surface area is found to be $100 \text{ m}^2/\text{g}$, the average pore radius is $r = 4.6 \text{ nm}$, and the pore volume is $0.218 \text{ cm}^3/\text{g}$. For such materials, the pore size distribution is generally narrow [43,44]. The ratio of the pore length to diameter lies between 5 and 7, and the sample porosity is $\varepsilon = 0.3$ [34]. The water sorption and desorption curves for such a material are provided by Gruener *et al.* [23]. We use samples with a main axis length of 1.2 cm and section of $4 \times 6 \text{ mm}^2$.

For drying experiments, we start by placing the dry sample in contact with distilled water, which ensures full saturation. Then, all the faces of the sample, except one (its “free surface”), are covered with Teflon, and the sample is submitted to a dry-air flux along this free surface (see inset of Fig. 1), which induces the transport of water along its main axis towards the free surface. The temperature is $(21 \pm 1)^\circ\text{C}$. The drying rate increases with the air-flux intensity, which may be understood as a result of the decrease of the thickness of the (boundary) layer of exchange, through which the vapor has to diffuse to reach the dry region. As we see in Sec. IV, the most straightforward way to characterize the air flux is through this layer thickness (δ), which can be estimated from the initial drying rate, i.e., when the sample is saturated. The sample is inserted into a Bruker NMR minispec mq20 instrument, 0.5 T. We measure the transverse relaxation time, T_2 , of water protons using a Carr-Purcell-Meiboom-Gill sequence [45] with the main following parameters: number of scans, 256; echo time, 0.4 ms (i.e., less than the minimum T_2 for adsorbed water); and repetition time,

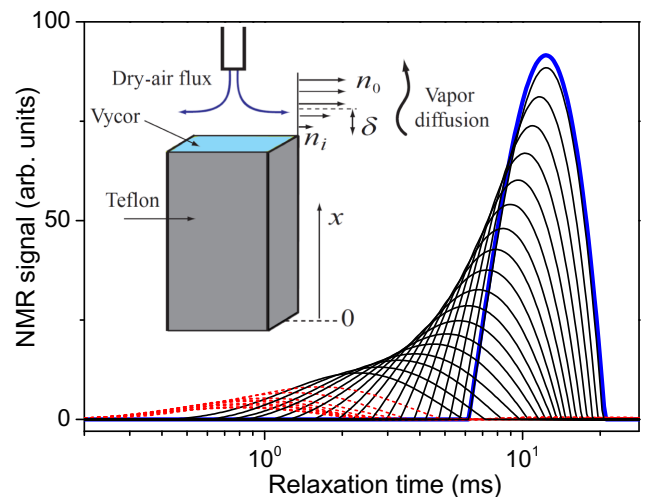


FIG. 1. Relaxation-time distribution for an intermediate air flux (see Sec. II) ($\delta = 8.5 \text{ mm}$) at different times during drying: every 3 h (continuous black lines), then every 6 h (dashed red lines). Initial distribution is the thick blue line. Inset shows a schematic of the experiment.

2 s, for a total measurement duration (for one T_2 distribution) of 5 min. Such data may be analyzed to obtain the probability density function (PDF) of the NMR relaxation time T_2 , which we call the relaxation-time distribution. Details of this technique and the physical interpretations are described elsewhere [46,47]. Roughly speaking, for such small pores, the relaxation time is related to the mobility of water molecules. More precisely, according to the Brownstein and Tarr model [48], under the assumption of biphasic fast exchange, the relaxation time scales with the ratio of the volume of free liquid water to the area of the water-solid interface, with a factor that depends on the interactions of the water molecules with the surface.

During the same tests, it is also possible to get, with the spin-echo sequence, 1D NMR profiles of the water content with this NMR system equipped with a 4 T/m vertical pulsed gradient unit. These 1D profiles obtained by Fourier transform represent the spatial distribution of water along the sample-drying axis, each data point corresponding to the free-water content in a cross-section layer of thickness equal to the spatial resolution. The main parameters used are number of scans, 256; echo time, 7.2 ms; field of view, 20 mm; number of pixels, 128; and repetition time, 2 s, for a total measurement duration of 5 min. However, in the present context, the profiles obtained from this procedure can be seen as qualitative because of the standard weighting of the signal amplitude in the spin-echo sequence by a factor $\exp -T_E/T_2$, in which T_E is the echo time and T_2 is the most representative transverse relaxation time of the slice. In other words, the NMR signal in these profiles may be affected by local relaxation, which is rather fast for water in such nanopores. The strong dependency of the relaxation time on saturation (Sec. III A) allows the development of a deweighting procedure to recover quantitative profiles (i.e., a local signal amplitude that is effectively proportional to the local water mass concentration). Toward this aim, we use the straightforward correspondence between T_2 and saturation in the case of a homogeneous desaturation of the sample under very slow drying conditions (Sec. III B), which allows the corresponding spin-echo weighting to be deduced for each layer at each time during drying. Note that, with this procedure, due to increasing noise for lower saturation, reliable data can be obtained only for a saturation larger than 0.25.

III. RESULTS AND DISCUSSION

A. General characteristics

A typical evolution of the relaxation-time distribution during drying is shown in Fig. 1. By integrating this distribution over the whole range of relaxation times, we obtain the total NMR signal over time, from which we can deduce the average saturation (as the ratio of the current to the initial total NMR signal, i.e., \bar{S}) versus time curve for our different experiments.

The qualitative evolution of the relaxation-time distributions is similar for all our experiments. The initial distribution, which corresponds to the sample saturated with water in the liquid state, exhibits only one relatively narrow symmetrical peak situated around a relaxation-time value of 12 ms. This single peak further supports the validity of the fast-exchange assumption [49], i.e., in which, thanks to self-diffusion, the water molecules reach the solid walls a large number of times during NMR relaxation, so that, according to the Brownstein and Tarr model [48], the relaxation time is proportional to the ratio of the liquid volume to the wetted surface area. Note that, since the typical length of diffusion of a water molecule over a time duration of 12 ms is in the order of 10 μm , the relaxation time results from an exploration of the medium over a distance much larger than the pore size, and thus, is related to the average volume-to-surface ratio well beyond the local heterogeneities. During drying, the amplitude of this peak decreases, as a result of the water content decreasing, and simultaneously the peak shifts towards shorter relaxation time. This is consistent with a fast-exchange situation, in which essentially the liquid volume decreases, while the wetted area does not vary significantly. More precisely, the average relaxation time of each distribution appears to evolve very similarly to the water content (see Fig. 2), which exactly corresponds to the prediction of the Brownstein and Tarr [48] model, assuming that the area of the solid-liquid interface remains essentially constant. Our observations thus demonstrate that the liquid wets most of the solid surface throughout the drying process.

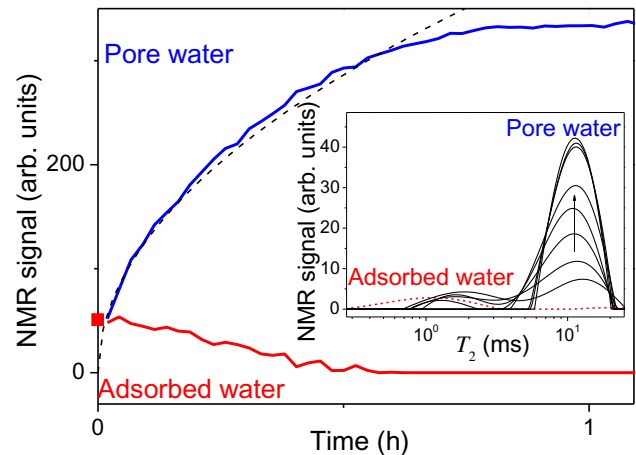


FIG. 2. Imbibition of a Vycor sample: water mass (proportional to the NMR signal) associated with each region of relaxation time, i.e., below (adsorbed water) or above (pore water) 4 ms, as deduced from the integral of the probability density function in these ranges. Black dashed line is the Washburn model fitted to data (see text). Inset shows the distributions of transverse relaxation time at different times during imbibition (black curves from bottom to top): 3, 6, 11, 19, 32, 49, 66, 75 min. Red dotted line is the initial distribution (before imbibition).

Finally, the distribution approaches a peak centered around 0.9 ms. It may nevertheless be noted that, during desaturation, there is also a progressive slight spreading of the peak, i.e., the width of the distribution increases, which suggests that some slight saturation heterogeneity also develops in the sample, leading to different T_2 in different parts of the sample.

It is worth noting that, in the last stage of drying, the average saturation slowly but continuously decreases towards lower values. At the end of our experiment, saturation, which is still decreasing, reaches a value in the order of 7%. Assuming a homogeneous layer covering the solid surface, this value equals the ratio of the specific area times the layer thickness to the pore volume. Under these conditions, the mean thickness would be 0.15 nm, about half the water molecule's diameter. This suggests that, in this stage, there is only partial coverage of the solid surface by water molecules.

It is also remarkable that when the sample in such a state is now placed again in contact with a liquid bath, which leads to progressive imbibition, the initial peak located around 1 ms progressively disappears as the sample is invaded by water, while a peak appears at much longer relaxation time, say around 10 ms (see inset of Fig. 2), the amplitude of which grows over time. This corresponds to the progressive penetration of water in the sample. Indeed, as soon as a pore is invaded by water, the water molecules initially adsorbed along the surface and exhibiting a short relaxation time are now just molecules among others in the pore; all the water molecules now take part in the fast-exchange process, leading to a single relaxation time, longer than that associated with surface relaxation.

We can further quantify this process through the integration of the PDF over the range of relaxation times, including this growing peak, i.e., say between 4 and 25 ms. The curve of the resulting signal as a function of time is typical of a diffusion or capillary imbibition process [21], i.e., with variation as a function of the square root of time (see Fig. 2). Remarkably, the relaxation time of pore water remains constant over time (see inset of Fig. 2). This confirms that water invades the medium by progressively fully saturating a region of increasing thickness. This is also confirmed by MRI measurements of 1D water-content profiles (see Appendix A). This process, in fact, corresponds well to capillary imbibition, as assumed in the Washburn model. The evolution of the signal associated with the initially adsorbed layer confirms this analysis: its amplitude progressively decreases as the signal of water at longer T_2 increases (see Fig. 2). Note that, although it corresponds to the noninvaded region, the adsorbed-water signal does not seem to decrease with the square root of time, as expected from the above analysis. This likely due to the uncertainty in measurements for such a low signal amplitude, and the impact, on the Laplace transform used to get the PDF, of

the presence of a nearby large peak associated with pore water.

B. Detailed drying characteristics

Differences in the drying characteristics appear when looking at the saturation against time curves (see Fig. 3). For sufficiently slow air flux, i.e., large δ (see definition in Sec. IV), the drying rate (i.e., water-mass loss per unit time), proportional to the slope of the saturation versus time curve, remains constant down to low saturation, then progressively decreases (see inset of Fig. 3). For stronger air flux, there also exists an initial period of constant drying rate, but this period extends over a shorter range of saturations as the air flux is increased.

These trends are associated with specific characteristics of the 1D profiles presented in Fig. 4(a). First note the consistency of these data with those extracted from the PDF: the saturation found by integration of the 1D profiles at different times corresponds to the saturation deduced from the integration of the distributions of relaxation time (see Fig. 3). Also note that these 1D profiles likely reflect a homogeneous situation in the radial direction. Indeed, significant edge effects are very unlikely, as they would barely allow perfectly homogeneous desaturation down to low values, as in Fig. 4(a): edge effects with different impact would occur at different depths in the sample, which are associated with different edge contexts.

For sufficiently weak air flux, rapidly after the beginning of the experiment, the 1D profiles exhibit a slight

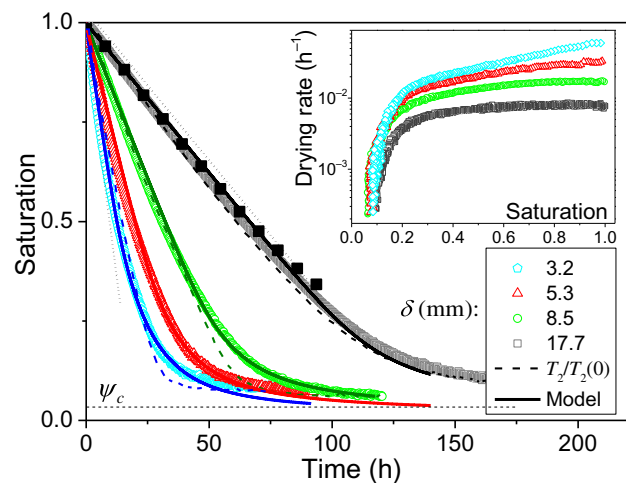


FIG. 3. Total water content over time during Vycor sample drying under different air fluxes (resulting in different boundary-layer thicknesses). Current-to-initial-relaxation-time ratio is represented for some tests (dashed lines). Black filled square symbols correspond to saturation computed from the 1D profiles shown in Fig. 4(a). Inclined straight dotted lines are guides for the eye. Inset shows the corresponding drying rate [saturation variation per unit time (in hours)] for different tests (same symbols and colors).

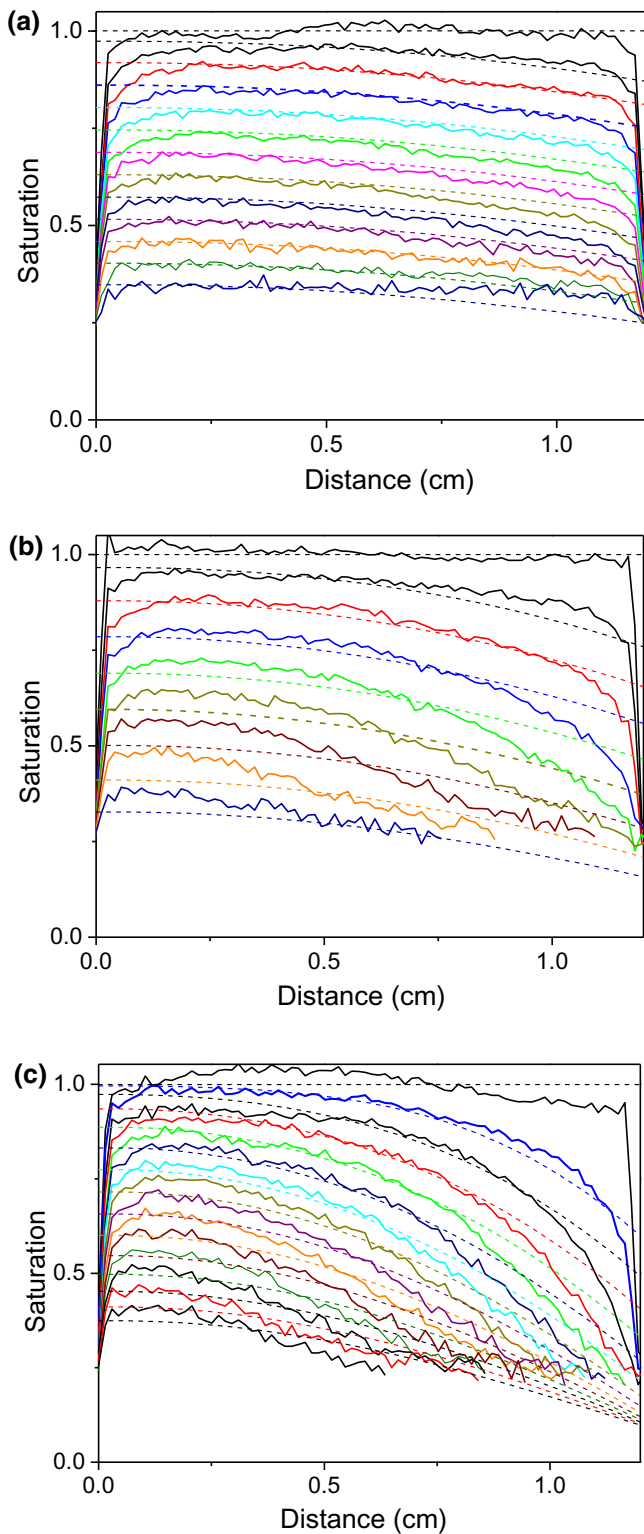


FIG. 4. Saturation distribution (1D profiles) along sample-drying axis at different times during drying with different air-flux intensities: (a) $\delta = 17.7$ mm, profiles every 7.8 h; (b) $\delta = 8.5$ mm, profiles every 6 h; (c) $\delta = 3.2$ mm, profiles every 1.5 h, from initial time. Continuous lines correspond to NMR measurements, dashed lines to model predictions. Note that here saturation is obtained by dividing the local NMR signal by the initial NMR signal averaged over the sample length.

slope and then remain parallel to each other [see Fig. 4(a)]. Thus, remarkably, during drying, (i) the nanoporous material starts to desaturate in depth while its mean saturation only slightly decreases, and (ii) no dry region develops below the free surface.

This is reminiscent of the drying characteristics of simple micro- or macroporous systems, typically bead packings [38], clay [36], or cellulose paste [50], for which saturation is observed to remain perfectly uniform down to a value of 30% or lower. This results from capillary effects able to establish, by inducing liquid transport, a saturation equilibrium throughout the sample, sufficiently rapidly with respect to the drying rate imposed by external conditions [51]. Note that, in channels of a few tens of nanometers (i.e., sufficiently larger than the critical size of nucleating vapor bubbles [52]), instead of the standard air-path propagation associated with capillary effects, cavitation is observed to be at the origin of a desaturation in depth (i.e., at some distance from the open surface of the sample) [52]. As for the standard capillary re-equilibration process, the air-liquid interface along the open surface of the sample remains almost the same. This situation allows a constant drying rate to be maintained, as constant humidity conditions are maintained in the sample and, in particular, along its free surface (i.e., around 100%) from which the vapor diffuses. Moreover, for such simple micro- or macroporous systems, when liquid transport induced by capillary effects is not sufficiently fast, with respect to the initially imposed extraction rate, because now the permeability is too low [51], a dry region starts to develop from the free surface. Then, the drying rate results from vapor diffusion, from the liquid-air interface now situated inside the medium, to the free surface. Note that this is an “apparently dry” region, since the saturation is here generally appreciated with respect to the saturation measured in the main wet region. For example, a nanolayer of liquid molecules covering the solid surface in the “dry” region can barely be detected with the technique used in such cases.

Here, we see that, for a nanoporous medium, despite a very low permeability (it scales with the square of the pore size), an almost homogeneous desaturation is maintained down to low (mean) saturation, and no dry region develops. Such a result is likely to be general for a nanoporous medium with a connected pore network, since it is also obtained with silica-bead packings for a single air flux and different bead sizes from 40 to 6 nm [38]. Moreover, here, no clear dry region tends to develop when the air-flux intensity is increased: now the slope of the saturation distribution becomes steeper at the approach of the sample’s free surface, and the overall slope increases for stronger air flux, but saturation still seems to tend to zero only at the approach of the free surface, even after significant drying [see Figs. 4(b) and 4(c)]. This suggests that the dominant physical effects at play during drying of a nanoporous

material differ from the usual effects taking place in porous materials with larger pores. More precisely, there need to be stronger forces maintaining contact between the liquid and the solid, but also allowing the liquid to flow through the sample sufficiently rapidly.

Furthermore, looking more globally at the saturation distribution over time (see Fig. 4), we can infer that these effects can lead to some diffusion process through the sample, resulting from some rate of extraction imposed at the boundary. Indeed, for a low rate of extraction, the liquid has time to almost uniformly distribute throughout the sample, but still some gradient of concentration should exist to induce a flow towards the boundary. For a larger extraction rate, this gradient of concentration has to be larger, and this effect is stronger at the approach of the region of liquid extraction.

Finally, if, in addition, we take into account both the above observations and studies on light [53–57] and neutron scattering [58], for a similar sample upon drying, we can conclude that the vapor phase invades according to an invasion percolation mechanism into the nanoporous medium, for which the interconnectivity of the pores plays an important role [59,60]. Additionally, a pore-network study of the Kelvin effect for drying of mesoporous materials offers reasonable arguments for a rapidly equilibrated drying process with homogeneous desaturation over time [61]. It is not sufficient for the humidity to be reduced below the pressure that drains a pore of a given radius; if this pore also has unrestricted access via a percolation path of empty pores to the surface, it can be emptied quickly. If it is blocked by smaller pores, it cannot drain until a sufficiently low value of humidity is reached to empty the narrowest blocking pores. As a result, the random connectivity leads to an interconnected disordered network (or cluster) of drained pores. Additionally, consider the liquid flow and coexistence of menisci with different curvatures, and thus, Laplace pressures. Menisci in large-pore segments are receding, since they have a larger curvature

radius, and thus, a smaller Laplace pressure counteracting the desaturation flux, i.e., the Laplace pressure at small menisci. These clusters soon reach sizes on the order of the visible-light length scale, i.e., fractions of a micrometer, so that strong light scattering is observable upon drying in the entire sample [53–57]. In fact, a detailed analysis of light scattering allows one to confirm predictions of the invasion percolation theory with regard to the vapor-cluster geometries, most prominently the determination of their fractal dimension, $d_f = 2.6$.

Of course, we have no direct evidence for this scenario; however, based on the rigorous neutron- and light-scattering analysis described above, we suggest, for our drying geometry, that percolating fingers of large empty pore clusters start from the surface and quickly reach the bottom of the sample, see the panel sequence (a) to (b) in Fig. 5. In this propagating mode (regime I), a small saturation gradient from the top to the bottom is present. As soon as the invasion percolation fingers reach the sample bottom, they laterally increase in size, so that a homogeneous desaturation of the sample takes place [see Figs. 5(c) and 5(d)] until the sample is completely dry, except for a few monolayers of water adsorbed at the pore surface in the entire sample.

In the following, we describe theoretically the processes, with the help of quantities, that must be understood as averages over sample volumes much larger than these heterogeneities. Note that the above description, in terms of percolating paths, suggests that a similar phenomenon would take place during a standard desorption experiment, so that, in fact, the desorption curve would not necessarily represent a homogeneous situation at a local scale.

IV. MODELING

Let us examine more precisely the physical effects taking place in this process, starting with the drying conditions imposed by air flux. Drying occurs as a result of some

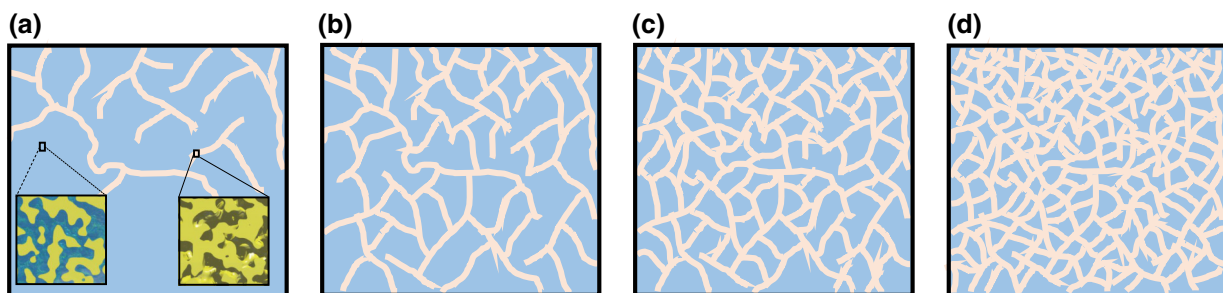


FIG. 5. Illustration of the drying process in nanoporous silica glass. Invasion percolation clusters of partially empty pore segments (blue) propagate from the top to the bottom (a),(b) through the saturated sample (yellow). Upon reaching the bottom, clusters increase homogeneously in size, resulting in a homogeneous desaturation (c),(d). Insets in (a) show detailed aspects of the structure at the pore scale (typical pore size about 10 nm) in two different regions (empty or saturated). Please note that the illustration of the desaturation process represents the authors’ naïve imagining of the invasion percolation process, as it is rigorously shown to occur in drying of Vycor by light- and neutron-scattering experiments [53–57].

imbalance between the humidity conditions inside the sample and the external conditions. Here, the imbalance is maintained by the dry air flux above the sample surface. Since the air flux can hardly penetrate the sample, which is a finely divided dead-end network, the air essentially steadily flows along this surface. For such an air flow along a wet surface, it may be shown, from the solution of the advection-diffusion equation, that along the normal direction above each point of the surface the gradient of RH (Relative Humidity), noted n , is almost constant, so that, as a first approximation, the vapor diffuses freely from the sample surface over a distance δ where it reaches the region where RH is equal to n_0 . The value of δ depends on the position along the sample surface, on the surface shape and size, and on the air-flux characteristics. It is then natural to assume that a single average value of δ , associated with given geometrical and kinematic conditions, allows the whole process of vapor transport above the sample surface to be represented [62,63]. It is worth emphasizing that, under these conditions, the drying rate results from the diffusion of vapor from the free surface, where RH is equal to n_i , to the distance δ , where RH is equal to n_0 (see the inset of Fig. 1); thus, δ is independent of the water-transport phenomena occurring inside the sample, and the drying rate depends only on these phenomena through the value n_i to which they lead. More precisely, according to Fick's law, in this boundary layer, the vapor flux, which is also the drying rate, may finally be written as $J_0 = -\rho_0 D_0 \nabla n$, where $\rho_0 = 0.0185 \text{ kg m}^{-3}$ is the saturation vapor density at our ambient temperature, $D_0 = 2.7 \times 10^{-5} \text{ m}^2 \text{ s}^{-1}$ is the coefficient of diffusion of vapor in air, and $\nabla n = \partial n / \partial x = (n_0 - n_i) / \delta$ (x is the distance along the direction of transport). δ can be directly estimated from the initial drying rate of the sample, since in this case n_i is known. Considering the desorption curve of the Vycor sample, here, n_i is initially equal to 1, but then we have a decrease of n_i towards 0.8 without a significant change in saturation, so that finally the initial drying rate deduced from our data is essentially associated with $n_i = 0.8$. The values for δ indicated in this paper are estimated in this way. Afterwards, i.e., during drying, the current drying rate will depend on the mechanism of water transport in the whole medium, leading to a value of n_i possibly varying over time.

A. Vapor transport

During drying, water is transported through the sample towards the free surface, and then diffuses in the form of vapor through the boundary layer. This internal transport can occur in the form of vapor diffusion or liquid flow. The vapor diffuses in the air network throughout the material as a result of some RH gradient, ∇n . Since the pore size is smaller than the mean free path of water molecules ($l \approx 100 \text{ nm}$ [64]), i.e., a large Knudsen

number (molecular regime), the diffusion coefficient is approximately $\varepsilon(1 - S)D_v/\tau$ [64], in which τ is the tortuosity of the void network in Vycor ($\tau \approx 3.5$ [23,65]), $\varepsilon(1 - S)$ is the volume fraction of the void network, and $D_v = 2rD_0/l$. The resulting mass flux is written as $J_v = -\rho_0(\varepsilon(1 - S)D_v/\tau)\nabla n$. Here, the gradient of n can be estimated from the 1D distributions of $S(x)$ and the desorption curve, assuming we have a local equilibrium situation, i.e., $n = n(S)$, at any time. This assumption seems realistic considering the very slow variations (slight changes of n over hours) of the local humidity with time during these drying tests. The validity of this assumption is checked in the case of cellulose-fiber drying [63]. Notably, from our data, the vapor mass flux estimated from the above equation appears to be much lower than the observed mass flux by a factor of several orders of magnitude. This means that the contribution of vapor flux due to the RH gradient inside the sample is negligible, with regard to vapor transport outside, in particular, just above the sample top. This implies that most of the water supplied for vapor transport in the boundary layer does not originate from vapor transport deep in the sample, but rather comes from the liquid situated close to the free surface of the sample. As a corollary, water transport inside the sample mainly occurs in the form of liquid flow until the water reaches the sample top and finally evaporates.

Moreover, we do not have information about the contact between Teflon and the Vycor sample, but (i) a liquid layer of thickness significantly larger than the pore size cannot exist, as it cannot be at equilibrium with the mean saturation in the sample and the corresponding Laplace pressure; and (ii) if a liquid layer of significant thickness forms, it will induce the presence of a small peak situated at longer T_2 in the PDF. Thus, if the contact with Vycor is imperfect, and leads to the existence of some layer of thickness larger than the pore size, this layer is *a priori* filled with vapor. As a consequence, water transport in this layer is associated with vapor transport, which can be estimated in the same way as for vapor transport through the porous structure (see above), so we can conclude it is negligible.

B. Liquid transport

Liquid motion in the porous medium results from some pressure gradient that comes from the gradient of saturation through the sample. For sufficiently large pore sizes, this induces a gradient of Laplace pressure due to capillary effects, as the meniscus size decreases for decreasing saturation [38]. Nevertheless, in that case, although we know that the Laplace pressure increases as the saturation decreases, the exact theoretical relationship between these two variables is extremely difficult to establish from wetting characteristics and geometrical considerations. As a consequence, we cannot predict exactly the rate of liquid transport due to capillary effects. The advantage of a nanoporous medium that saturates when submitted to

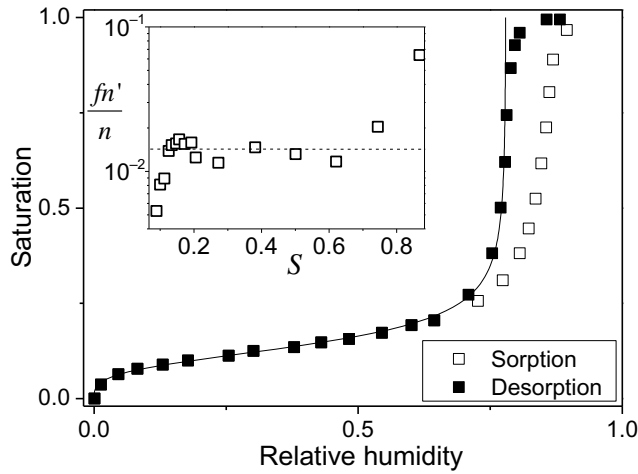


FIG. 6. Water sorption and desorption curves of the Vycor sample. Inset shows the value of the saturation-dependent parameter of the diffusion coefficient computed from the desorption curve and the empirical model for permeability of the partially saturated porous medium.

a RH increased up to 100% is that, for a process like drying, during which saturation decreases over time, the relationship between the pressure in the liquid and saturation can be directly derived from the desorption curve, i.e., $S(n)$ (see Fig. 6). Moreover, considering the slow variations of saturation with time (over hours), the local saturation and liquid-air interface are at equilibrium with the surrounding vapor at any time and position inside the medium. Indeed, since the velocity of vapor molecules is in the order of 400 m/s (as deduced from the expression of thermal energy as the mean kinetic energy of the particles), while the pore size is a few nanometers, the time needed for a vapor molecule to reach a liquid layer along a wall is in the order of 10^{-11} s. This time is then also the characteristic time for an elementary exchange between vapor molecules and a molecule of the liquid phase. The volume of a pore is in the order of 4^3 nm^3 , so the maximum number of water molecules (of volume 0.34^3 nm^3) is $(4/0.34)^3$, i.e., in the order of 1600. The maximum time for complete exchange of the water molecules in the liquid phase is thus less than $10^{-11} \times 1600$, i.e., less than 10^{-8} s, which is well below the characteristic time of variation of the local saturation, which is derived from the characteristic time of drying (hours). This implies equality between the pressure, P_L , in the liquid and the vapor water potential, i.e., $(RT/\Omega_m) \ln n$, which gives the so-called Kelvin equation:

$$P_L = (RT/\Omega_m) \ln n(S), \quad (1)$$

in which $\Omega_m = 18 \text{ cm}^3 \text{ mol}^{-1}$ is the molar volume of the liquid and R is the molar gas constant ($R = 8.31 \text{ J K}^{-1} \text{ mol}^{-1}$).

To describe the flow of the liquid network through the structure, we can write Darcy's law, which relates the pressure gradient to the flow rate, i.e., $\nabla P_L = \mu V/k$, in which μ is the liquid viscosity, k is the permeability of the medium, and V is the mean velocity through the structure (i.e., the ratio of the liquid flow rate per sample cross-section area). The permeability of the partially saturated medium may be expressed as $k = k_0 f(S)$, in which k_0 is the permeability of the saturated medium ($S = 1$), and f is a function decreasing from 1 to 0 as S decreases to 0.

Taking the gradient of Laplace pressure into account, Darcy's law for the liquid network is written as

$$\frac{\mu}{k_0 f(S)} V = \frac{RT}{\Omega_m} \nabla (\ln n(S)) = \frac{RT}{\Omega_m} \frac{n'(S)}{n(S)} \nabla (S). \quad (2)$$

We deduce an equation for the water volume concentration in the sample, i.e., $\varphi = \varepsilon S$, where ε is the porosity, similar to Fick's first law, $V = -D \nabla \varphi$, with

$$D(S) = \frac{k_0 RT f n'}{\varepsilon \mu \Omega_m n}. \quad (3)$$

Fick's second law for φ , from which we directly get a diffusionlike equation for S (the mass flux is $J = -\rho D \nabla S$), states

$$\frac{\partial S}{\partial t} = \nabla (D \nabla S). \quad (4)$$

Thus, we expect the drying characteristics to be the result of a process described by a nonlinear diffusionlike transport equation, with an effective-diffusivity coefficient that depends on the local saturation value, and boundary conditions evolving with saturation around the free surface, as above described. Note that similar equations for unsaturated transport in porous media are obtained, with analogous principles of derivation, e.g., the well-known Richards equation [66], or different approaches developed for cementitious materials [64] and for textiles [63] that take into account both vapor and liquid transport through porous systems. The specificity of our approach is the quantification of the Laplace pressure variations through the sorption curve.

Actually, we can estimate the value of the saturation-dependent factor $f n'/n$ from the slope of the desorption curve and using a power-law model for the permeability of partially saturated porous media, i.e., $f = (S - S_c)^3 / (1 - S_c)^3$, in which S_c corresponds to some residual liquid layer. Here, in view of all our data, we take $S_c = 0.035$, which appears to be the minimum saturation level reached during drying tests (see Fig. 3), and thus, corresponds to this residual liquid layer. Such an expression is most frequently assumed in the literature; in particular, it corresponds to that proposed to represent a wide set of experimental data [67] and is close to various

other theoretical expressions [68]. Moreover, it represents existing data very well for bead or granular packings (see Ref. [69]). One may remark that the structure of the Vycor porosity, which differs from that of granular packing, might induce some different trends, but we are not aware of existing data for that system. However, the validity of the model for a wide range of materials, either monodisperse or polydisperse, thus exhibiting different porous structures, suggests it can reasonably be extended to the Vycor structure. Finally, from abovementioned data, we can suggest that the uncertainty associated with the use of this model is less than 20% for a saturation higher than 0.4, but significantly increases as the saturation decreases to the critical value.

Under these conditions, it appears that, despite the strong variations of n and f over the whole range of saturations, the factor fn'/n remains approximately constant for S in the range of 0.1–0.8 (see inset of Fig. 6), i.e., we have $fn'/n \approx (0.0145 \pm 35)\%$. This means that a good approximation of the process can be obtained by using a constant diffusion coefficient in Eq. (3).

Additionally, we can estimate k_0 from the imbibition test (see Fig. 2). Indeed, in that case, we have a saturating front advancing in the medium, at a height h as a function of time t , given by the Lucas-Washburn model [21], $h = 2\sqrt{k_0 t \sigma \cos \theta / \epsilon r \mu}$, in which σ is the surface tension and θ is the contact angle. Note that here we estimate the Laplace pressure to be due to a meniscus of radius r at any time, which is a critical simplification. We also assume perfect hydrophilicity, i.e., $\theta = 0$. This can be justified since the contact angle enters with the cosine into the Lucas-Washburn equation. Even if θ deviates from zero ($\cos \theta = 1$), a contact angle of up to 25° , as reported for silica surfaces that are not specifically cleaned, would only change the result of the cosine to a value of 0.9. Fitting this curve to data, assuming the sample top ($h = 1.2$ cm) is reached at the plateau of the NMR signal (see Fig. 2), we find that $K = k_0 \sigma / \epsilon r \mu \approx 14.3 \times 10^{-9} \text{ m}^2 \text{ s}$, from which we deduce $k_0 \approx 2.7 \times 10^{-19} \text{ m}^2$, with an uncertainty in the order of 2%. Such a value is consistent with previous observations, based on gravimetric imbibition experiments [42], on a similar Vycor sample, leading to a hydrodynamic tortuosity of 3.6; the permeability can then be approximated by $k_0 = r^2 \epsilon / 8 \tau$, resulting in 2.2×10^{-19} , which is close to the value inferred in our analysis.

Finally, from Eq. (3), we get $D(S) \approx 1.8 \times 10^{-9} \text{ m}^2 \text{ s}^{-1}$. Remarkably, this value is close to the almost-constant value obtained by Page *et al.* [54] through a different approach for hexane desorption from Vycor.

The predictions of this simple model, i.e., Eq. (3) with the boundary conditions $J(x=H) = \rho_0 D_0 n_i(S) / \delta$ and $J(x=0) = 0$, can be computed by a simple finite-element method. Note that the solution can also be expressed in an analytical form (see Crank [70], equation 4.53). With this aim, we use an empirical model to represent the desorption curve [i.e., $n(S) = (1.3 + 0.0013S^{-3.5})^{-1}$] (see

Fig. 6). After adjusting the value of the effective diffusivity to a slightly lower value, i.e., $D = 1.3 \times 10^{-9} \text{ m}^2 \text{ s}^{-1}$, we observe excellent agreement between these predictions and our data. This discrepancy between the theoretical and measured values of diffusivity can come from the simplifying assumptions made concerning the wetting characteristics, i.e., the contact angle and the meniscus radius (see above), in the analysis of the imbibition process to estimate (saturated) permeability. First of all, the whole set of drying curves, i.e., in a wide range of air fluxes, are well represented by the model (see Fig. 3). Moreover, the theoretically calculated water distributions with time represent data obtained under these different conditions very well and lead to either slight or strong saturation gradients (see Fig. 4). Nevertheless, in some cases, the slope of the theoretical profiles at the approach of the free surface is less prominent than it appears from data. This may originate from the uncertainty of the desorption measurements and representation by a model, the error introduced in the model by assuming a constant diffusion coefficient, and in the uncertainty of the permeability function model. It seems difficult to elaborate further, in particular, quantitatively, about the origin of this discrepancy. However, we can add that, despite this discrepancy, all qualitative features are well predicted by the model under different air fluxes and, even more remarkable, the model predicts the drying rate very well over the whole range of saturation in any case (see Fig. 3), which further supports its predictive nature.

V. CONCLUSION

Our results show that water transport in silica glass is mainly ensured by liquid flow resulting from a gradient of vapor pressure, assuming otherwise standard hydrodynamic characteristics. The resulting simple diffusionlike model, assuming a constant effective-diffusivity-coefficient value, appears to represent data very well in terms of the spatial distribution of water over time inside the sample for various boundary conditions (air-flux intensities) and at different saturations. This tends to validate our physical interpretation of the physics of drying of such a nanoporous medium, which can be generalized to other nanoporous media. For example, since the 1D profiles observed for a given air flux and beads of different nanometric sizes are similar [1,38], we expect that the same modeling approach can be applied to granular packing too. Finally, we propose a predictive model of the detailed drying characteristics of a nanomaterial from knowledge of its pore size, permeability, and desorption curve.

It is worth noting that our description is valid at a scale larger than the heterogeneities developing in the system, i.e., the probable air paths resulting from invasion percolation processes. This means that the desorption process does not take place homogeneously in all pores, and we cannot

see desaturation and the resulting two-phase flow as taking place similarly in all pore sizes at the same time.

Let us note that such results could be essential for applications in the field of energy: good control and prediction of water transfer inside the material allows, possibly with some coupling, the dynamics and distribution of thermal transfers in the medium, associated with latent heat, to be deduced, opening the way to a full physical approach to heat and mass transfer in nanoporous materials.

ACKNOWLEDGMENTS

We acknowledge scientific exchange and support from the Center for Molecular Water Science (CMWS). P.H. acknowledges funding from the European Innovation Council (EIC) under the European Union’s Horizon 2020 research and innovation programme under Grant No. 964524 EHAWEDRY: “Energy harvesting via wetting-drying cycles with nanoporous electrodes” (H2020-FETOPEN-1-2021-2025). This work was also supported by the Deutsche Forschungsgemeinschaft (DFG) within

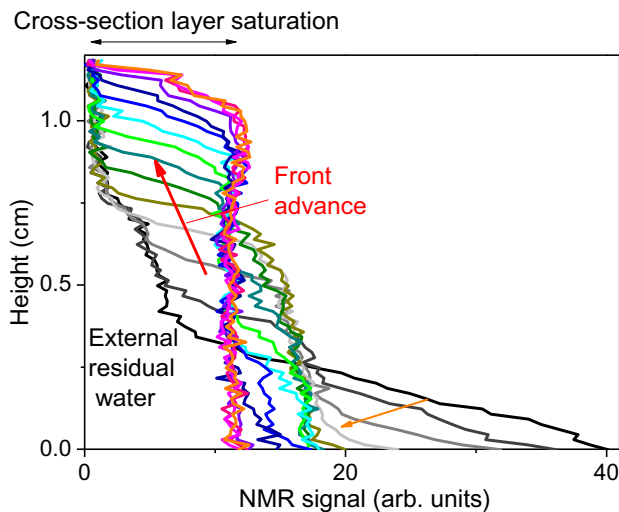


FIG. 7. Successive 1D profiles (distributions) of water over time (every 150 s) along the axis of a Vycor sample initially dry and partially immersed in a water volume. Each data point at a given height corresponds to the total water content in the cross-section layer around this height. As a consequence, this includes water inside the sample and (external) water between Teflon and the tube. As imbibition progresses, a (slightly inclined) front associated with sample saturation advances upwards, while the volume of external water decreases. In the final stage, there is no more external water and the sample is saturated all along its height (vertical 1D profile). Note that, for these tests, the time schedule for the early times is not well controlled, and the adsorbed monolayer cannot be observed due to its short relaxation time, which, in our opinion, precludes a detailed quantitative study of the process from such data in the present context.

the Collaborative Research Centre CRC 986 “Tailor-Made Multi-Scale Materials Systems” Project number 192346071.

APPENDIX A: 1D PROFILES DURING THE IMBIBITION PROCESS

In Fig. 7, we show the 1D profiles measured by the same MRI technique as that used for drying (see text). Here, it is worth noting that the profiles correspond to the distribution of all water content in successive layers at increasing depth. As a consequence, in the bottom region, the water content includes the water in the bath in which the sample is partially immersed (see inset of Fig. 7).

- [1] J. Thiery, S. Rodts, E. Keita, X. Chateau, P. Faure, D. Courtier-Murias, T. E. Kodger, and P. Coussot, Water transfer and crack regimes in nanocolloidal gels, *Phys. Rev. E* **91**, 042407 (2015).
- [2] J. Thiery, E. Keita, S. Rodts, D. Courtier Murias, T. Kodger, A. Pegoraro, and P. Coussot, Drying kinetics of deformable and cracking nano-porous gels, *Eur. Phys. J. E* **39**, 117 (2016).
- [3] S. D. Beyea, B. J. Balcom, T. W. Brenner, P. J. Prado, A. R. Cross, R. L. Armstrong, and P. E. Grattan-Bellew, The influence of shrinkage-cracking on the drying behaviour of white Portland cement using single-point imaging (SPI), *Solid State Nuclear Magn. Reson.* **13**, 93 (1998).
- [4] Y. P. Xi, Z. P. Bazant, L. Molina, and H. M. Jennings, Moisture diffusion in cementitious materials – moisture capacity and diffusivity, *Adv. Cem. Based Mater.* **1**, 258 (1994).
- [5] M. Woloscyn and C. Rode, Tools for performance simulation of heat, air and moisture conditions of whole buildings, *Build. Simul.* **1**, 5 (2008).
- [6] B. Bao, J. Qiu, F. Liu, Q. Fan, W. Luo, and S. Zhao, Capillary trapping induced slow evaporation, *J. Pet. Sci. Eng.* **196**, 108084 (2021).
- [7] W. Shi, R. M. Dalrymple, C. J. McKenny, D. S. Morrow, Z. T. Rashed, D. A. Surinach, and J. B. Boreyko, Passive water ascent in a tall scalable synthetic tree, *Sci. Rep.* **10**, 230 (2020).
- [8] O. Vincent, B. Marguet, and A. D. Stroock, Imbibition triggered by capillary condensation in nanopores, *Langmuir* **33**, 1655 (2017).
- [9] P. Huber, Soft matter in hard confinement: Phase transition thermodynamics, structure, texture, diffusion and flow in nanoporous media, *J. Phys.: Condens. Matter* **27**, 103102 (2015).
- [10] A. Davoodabadi and H. Ghasemi, Evaporation in nano/molecular materials, *Adv. Colloid Interface Sci.* **290**, 102385 (2021).
- [11] I. Burgert and P. Fratzl, Actuation systems in plants as prototypes for bioinspired devices, *Philos. Trans. R. Soc., A* **367**, 1541 (2009).
- [12] G. Y. Gor, L. Bertinetti, N. Bernstein, T. Hofmann, P. Fratzl, and P. Huber, Elastic response of mesoporous silicon to capillary pressures in the pores, *Appl. Phys. Lett.* **106**, 1 (2015).

- [13] R. Piotrowska, T. Hesketh, H. Wang, A. R. G. Martin, D. Bowering, C. Zhang, C. T. Hu, S. A. McPhee, T. Wang, Y. Park, *et al.*, Mechanistic insights of evaporation-induced actuation in supramolecular crystals, *Nat. Mater.* **20**, 403 (2021).
- [14] L. Bocquet and E. Charlaix, Nanofluidics, from bulk to interfaces, *Chem. Soc. Rev.* **39**, 1073 (2010).
- [15] U. Raviv, S. Giasson, J. Frey, and J. Klein, Viscosity of ultra-thin water films confined between hydrophobic or hydrophilic surfaces, *J. Phys.: Condens. Matter* **14**, 9275 (2002).
- [16] N. Kavokine, R. R. Netz, and L. Bocquet, Fluids at the nanoscale: From continuum to sub-continuum transport, *Annu. Rev. Fluid Mech.* **53**, 377 (2021).
- [17] P. Debye and R. L. Cleland, Flow of liquid hydrocarbons in porous Vycor, *J. Appl. Phys.* **30**, 843 (1959).
- [18] B. Abeles, L. F. Chen, J. W. Johnson, and J. M. Drake, Capillary condensation and surface flow in microporous Vycor glass, *Isr. J. Chem.* **31**, 99 (1991).
- [19] J. Zhong, M. A. Alibakhshi, Q. Xie, J. Riordon, Y. Xu, C. Duan, and D. Sinton, Exploring anomalous fluid behavior at the nanoscale: Direct visualization and quantification via nanofluidic devices, *Acc. Chem. Res.* **53**, 347 (2020).
- [20] O. Vincent, A. Szenicer, and A. D. Stroock, Capillary-driven flows at the continuum limit, *Soft Matter* **12**, 6656 (2016).
- [21] E. W. Washburn, The dynamics of capillary flow, *Phys. Rev.* **17**, 273 (1921).
- [22] P. Huber, S. Grüner, C. Schäfer, K. Knorr, and A. V. Kityk, Rheology of liquids in nanopores: A study on the capillary rise of water, *n*-hexadecane and *n*-tetracosane in mesoporous silica, *Eur. Phys. J.: Spec. Top.* **141**, 101 (2007).
- [23] S. Gruener, T. Hofmann, D. Wallacher, A. V. Kityk, and P. Huber, Capillary rise of water in hydrophilic nanopores, *Phys. Rev. E* **79**, 067301 (2009).
- [24] B. Coasne, Multiscale adsorption and transport in hierarchical porous materials, *New J. Chem.* **40**, 4078 (2016).
- [25] K. Falk, B. Coasne, R. Pellenq, F. J. Ulm, and L. Bocquet, Subcontinuum mass transport of condensed hydrocarbons in nanoporous media, *Nat. Commun.* **6**, 6949 (2015).
- [26] Y. Akkus, Modeling of evaporation from nanoporous membranes using molecular dynamics simulation, *Isi Bilim Ve Teknigi Dergisi-J. Therm. Sci. Technol.* **39**, 91 (2019).
- [27] P. Jain, O. Vincent, and A. D. Stroock, Adsorption, desorption, and crystallization of aqueous solutions in nanopores, *Langmuir* **35**, 3949 (2019).
- [28] W. Shi, J. Vieitez, A. S. Berrier, M. W. Roseveare, D. A. Surinach, B. R. Srijanto, C. P. Collier, and J. B. Boreyko, Self-stabilizing transpiration in synthetic leaves, *ACS Appl. Mater. Interfaces* **11**, 13768 (2019).
- [29] Y. Li, H. Chen, S. Xiao, M. A. Alibakhshi, C. W. Lo, M. C. Lu, and C. Duan, Ultrafast diameter-dependent water evaporation from nanopores, *ACS Nano* **13**, 3363 (2019).
- [30] Q. Xie, S. Xiao, and C. Duan, Geometry-dependent drying in dead-end nanochannels, *Langmuir* **33**, 8393 (2017).
- [31] A. Jatukaran, J. Zhing, A. H. Persad, Y. Xu, F. Mostowfi, and D. Sinton, Direct visualization of evaporation in a two-dimensional nanoporous model for unconventional natural gas, *ACS Appl. Nano Mater.* **1**, 1332 (2018).
- [32] D. Wallacher, N. Künzner, D. Kovalev, N. Knorr, and K. Knorr, Capillary Condensation in Linear Mesopores of Different Shape, *Phys. Rev. Lett.* **92**, 195704 (2004).
- [33] R. Valiullin, S. Naumov, P. Galvosas, J. Kärger, H.-J. Woo, F. Porcheron, and P. A. Monson, Exploration of molecular dynamics during transient sorption of fluids in mesoporous materials, *Nature* **443**, 965 (2006).
- [34] S. Gruener, Z. Sadjadi, H. E. Hermes, A. V. Kityk, K. Knorr, S. U. Egelhaaf, H. Rieger, and P. Huber, Anomalous front broadening during spontaneous imbibition in a matrix with elongated pores, *Proc. Nat. Acad. Sci. U. S. A.* **109**, 10245 (2012).
- [35] J. Van Brakel, Mass transfer in convective drying, *Adv. Drying* **1**, 217 (1980).
- [36] P. Faure and P. Coussot, Drying of a model soil, *Phys. Rev. E* **82**, 036303 (2010).
- [37] M. D. Seck, M. Van Landeghem, P. Faure, S. Rodts, P. Cavalier, R. Combes, E. Keita, and P. Coussot, The mechanisms of plaster drying, *J. Mat. Sci.* **50**, 2491 (2015).
- [38] J. Thiery, S. Rodts, D. A. Weitz, and P. Coussot, Drying regimes in homogeneous porous media from macro- to nanoscale, *Phys. Rev. Fluids* **2**, 074201 (2017).
- [39] L. Pel, H. Brocken, and K. Kopinga, Determination of moisture diffusivity in porous media using moisture concentration profiles, *Int. J. Heat Mass Transfer* **39**, 1273 (1996).
- [40] G. H. A. van der Heijden, L. Pel, H. P. Huinink, and K. Kopinga, Moisture transport and dehydration in heated gypsum, an NMR study, *Chem. Eng. Sci.* **66**, 4241 (2011).
- [41] P. Levitz, Porous Vycor glass: The microstructure as probed by electron microscopy, direct energy transfer, small-angle scattering, and molecular adsorption, *J. Chem. Phys.* **95**, 6151 (1991).
- [42] S. Gruener, PhD thesis, Saarland University, 2010.
- [43] A. B. Shelekhin, S. Pien, and Y. H. Ma, Permeability, surface-area, pore volume and pore-size of Vycor glass membrane heat-treated at high temperature, *J. Membr. Sci.* **103**, 39 (1995).
- [44] P. Levitz, Off-lattice reconstruction of porous media: Critical evaluation, geometrical confinement and molecular transport, *Adv. Colloid Interface Sci.* **76–77**, 71 (1998).
- [45] H. Y. Carr and E. M. Purcell, Effects of diffusion on free precession in nuclear magnetic resonance experiments, *Phys. Rev.* **94**, 630 (1954).
- [46] H. Penvern, M. Zhou, B. Maillat, D. Courtier-Murias, M. Scheel, J. Perrin, T. Weitkamp, S. Bardet, S. Caré, and P. Coussot, How Bound Water Regulates Wood Drying, *Phys. Rev. Appl.* **14**, 054051 (2020).
- [47] T. Lerouge, B. Maillat, D. Courtier-Murias, D. Grande, B. Le Droumaguet, O. Pitois, and P. Coussot, Drying of a Compressible Biporous Material, *Phys. Rev. Appl.* **13**, 044061 (2020).
- [48] K. R. Brownstein and C. E. Tarr, Spin-lattice relaxation in a system governed by diffusion, *J. Magn. Reson.* **26**, 17 (1977).
- [49] A. Valori, P. J. McDonald, and K. L. Scrivener, The morphology of C-S-H: Lessons from ^1H nuclear magnetic resonance relaxometry, *Cem. Concr. Res.* **49**, 65 (2013).

- [50] N. Ben Abdelouahab, A. Gossard, X. Ma, H. Dialla, B. Maillet, S. Rodts, and P. Coussot, Understanding mechanisms of drying of a cellulose slurry by magnetic resonance imaging, *Cellulose* **28**, 5321 (2021).
- [51] P. Coussot, Scaling approach of the convective drying of a porous medium, *Eur. Phys. J. B* **15**, 557 (2000).
- [52] C. Duan, R. Karnik, M. C. Lu, and A. Majumdar, Evaporation-induced cavitation in nanofluidic channels, *Proc. Natl. Acad. U. S. A.* **109**, 3688 (2012).
- [53] J. H. Page, J. Liu, B. Abeles, H. W. Deckman, and D. A. Weitz, Pore-Space Correlations in Capillary Condensation in Vycor, *Phys. Rev. Lett.* **71**, 1216 (1993).
- [54] J. H. Page, J. Liu, B. Abeles, E. Herbolzheimer, H. W. Deckman, and D. A. Weitz, Adsorption and desorption of a wetting fluid in Vycor studied by acoustic and optical techniques, *Phys. Rev. E* **52**, 2763 (1995).
- [55] S. Ogawa and J. Nakamura, Hysteretic characteristics of $1/\lambda^4$ scattering of light during adsorption and desorption of water in porous Vycor glass with nanopores, *J. Opt. Soc. Am. A* **30**, 2079 (2013).
- [56] S. Ogawa, $1/\lambda^4$ scattering of light during the drying process in porous Vycor glass with nano-sized pores, *J. Opt. Soc. Am. A* **30**, 154 (2013).
- [57] S. Ogawa and J. Nakamura, Optically observed imbibition and drainage of wetting fluid in nanoporous Vycor glass, *J. Opt. Soc. Am.* **32**, 2397 (2015).
- [58] J. C. Li, D. K. Ross, L. D. Howe, K. L. Stefanopoulos, J. P. A. Fairclough, R. Heenan, and K. Ibel, Small-angle neutron-scattering studies of the fractal-like network formed during desorption and adsorption of water in porous materials, *Phys. Rev. B* **49**, 5911 (1994).
- [59] D. Wilkinson and J. F. Willemsen, Invasion percolation: A new form of percolation theory, *J. Phys. A: Math. Gen.* **16**, 3365 (1983).
- [60] M. Prat, Isothermal drying of non-hygroscopic capillary-porous materials as an invasion percolation process, *Int. J. Multiphase Flow* **2**, 875 (1995).
- [61] O. Maalal, M. Prat, and D. Lasseux, Pore network model of drying with Kelvin effect, *Phys. Fluids* **33**, 027103 (2021).
- [62] M. Cocusse, M. Rosales, B. Maillet, R. Sidi-Boulenouar, E. Julien, S. Caré, and P. Coussot, Two-step diffusion in cellular hygroscopic (plant-like) materials, *Sci. Adv.* **8**, eabm7830 (2022).
- [63] X. Ma, B. Maillet, L. Brochard, O. Pitois, R. Sidi-Boulenouar, and P. Coussot, Vapor-Sorption Coupled Diffusion in Clothes Revealed by MRI, *Phys. Rev. Appl.* **17**, 024048 (2022).
- [64] J. F. Daian, *Equilibrium and transfer in porous media 1 – Equilibrium states* (Wiley, New York, 2014).
- [65] S. Gruener, D. Wallacher, S. Greulich, M. Busch, and P. Huber, Hydraulic transport across hydrophilic and hydrophobic nanopores: Flow experiments with water and *n*-hexane, *Phys. Rev. E* **93**, 013102 (2016).
- [66] L. A. Richards, Capillary conduction of liquids through porous mediums, *Physics* **1**, 318 (1931).
- [67] S. Irmay, On the hydraulic conductivity of unsaturated soils, *Trans., Am. Geophys. Union* **35**, 463 (1954).
- [68] S. Assouline and D. Or, Conceptual and parametric representation of soil hydraulic properties: A review, *Vadose J.* **12**, 1 (2013).
- [69] R. Yang, E. Lemarchand, T. Fen-Chong, and K. Li, Prediction of permeability of monodisperse granular materials with a micromechanics approach, *J. Appl. Geophys.* **127**, 82 (2016).
- [70] J. Crank, *The Mathematics of Diffusion* (Oxford Science Publications, Oxford, 2011), 2nd ed.